The role of local density in the collisional deactivation of vibrationally highly excited azulene in supercritical fluids

D. Schwarzer, J. Troe, and M. Zerezke

Citation: The Journal of Chemical Physics **107**, 8380 (1997); doi: 10.1063/1.475038
View online: http://dx.doi.org/10.1063/1.475038
View Table of Contents: http://scitation.aip.org/content/aip/journal/jcp/107/20?ver=pdfcov
Published by the AIP Publishing

The role of local density in the collisional deactivation of vibrationally highly excited azulene in supercritical fluids

D. Schwarzer, J. Troe, and M. Zerezke
Max-Planck-Institut für biophysikalische Chemie, Am Faßberg, D-37077 Göttingen, Germany

(Received 15 July 1997; accepted 19 August 1997)

The collisional deactivation of vibrationally highly excited azulene was studied from gas into compressed liquid phase by pump-and-probe picosecond laser spectroscopy. Collisional deactivation rates were compared with solvatochromic shifts $\Delta\nu$ of the azulene $S_3 \leftarrow S_0$ absorption band under identical conditions. Employing supercritical fluids at pressures between 0.03 and 4000 bars and temperatures between 298 and 640 K, measurements covering the complete gas–liquid transition were performed. For the energy transfer experiments, azulene with an energy of $\sim 20000\ \mathrm{cm}^{-1}$ was generated by laser excitation into the S_1- and internal conversion to the S_0^*-ground state. The subsequent loss of vibrational energy was monitored by following the transient absorption at the red wing of the $S_3 \leftarrow S_0$ absorption band near 290 nm. Transient signals were converted into energy-time profiles using hot band absorption coefficients from shock wave experiments for calibration and accounting for solvent shifts of the spectra. Under all conditions, the energy decays were found to be exponential with phenomenological deactivation rate constants k_c. k_c and spectral shifts $\Delta\nu$ showed quite similar density dependences: the low pressure linear increase of both quantities with density ρ at higher densities starts to level off, before it finally becomes stronger again. The parallel behavior of energy transfer rate constants and solvent shifts becomes particularly apparent near to the critical point: measurements in propane at 3 K above the critical temperature showed that k_c and $\Delta\nu$ are essentially constant over a broad density interval near to the critical density. These observations suggest that both quantities are determined by the same local bath gas density around the azulene molecule. By Monte Carlo simulations it is shown that $k_c(\rho)$ follows an isolated binary collision (IBC) model, if the collision frequency Z is related to the radial distribution function $g(r)$ of an attractive hard-sphere particle in a Lennard-Jones fluid. Within this model, average energies $\langle \Delta E \rangle$ transferred per ethane–azulene collision are temperature independent between 298 and 640 K and pressure independent between 0.03 and 4000 bars. By means of radial distribution functions the density dependence of $\Delta\nu$ can be represented as well. © *1997 American Institute of Physics.* [S0021-9606(97)01344-5]

I. INTRODUCTION

Collisional energy transfer of vibrationally highly excited molecules is of great importance for understanding many gas phase reactions. Therefore, considerable effort has been expended over the last decade to obtain detailed information about this process. In particular, direct time-resolved experiments have been performed employing spectroscopic techniques.[1,2] Activated molecules often were prepared by light absorption into electronically excited states undergoing fast internal conversion to the electronic ground state. The subsequent decay of vibrational energy was monitored by time resolved UV absorption,[3–6] IR emission,[7,8] energy-selective photoionization,[9] or by other techniques. By means of calibrated UV absorption coefficients, IR emission intensities, or ionization quantum yields, the transient signals led to the average energy $\langle \Delta E \rangle$ transferred per collision and its energy dependence.[10] Though not all details of the observed vibrational energy transfer in the gas phase are understood, considerable progress towards its quantitative characterization could be achieved.[11–14]

Collisional energy transfer of vibrationally highly excited polyatomic molecules in the liquid phase was studied far less extensively[15–22] with less clear results. For this reason, we recently studied the collisional deactivation of azulene with an initial internal energy of $19\,000\ \mathrm{cm}^{-1}$ from the gas to the compressed liquid phase in a variety of supercritical solvents.[23] It was shown that collisional deactivation rate constants k_c in helium linearly depend on density up to at least 16 mol/ℓ. For other collider gases like xenon, CO_2, and ethane, this linearity was only found up to densities of about 1 mol/ℓ. At higher densities the increase of the energy transfer rate slows down. These observations appear to be of more general significance because recent studies with excited cycloheptatriene[24] led to quite similar results.

For xenon, CO_2, and ethane, deviations of k_c from linearly extrapolated gas phase values were observed to occur at collision frequencies near to $Z = 0.3\ \mathrm{ps}^{-1}$.[23] Since $1/Z$ is of the same order of magnitude as the lifetime of collision complexes, it was suggested[23] that a reduction of the effective collision frequency by shielding of the excited molecule through collision partners might be the reason for the comparably low deactivation rate constants at high densities. The assumption that no energy transfer occurs in a collision of a bath gas molecule with excited azulene at a site which is occupied by another collider, and estimation of the fractional coverage of azulene with a simple Langmuir adsorption iso-

therm model, led to a surprisingly successful description of the collisional deactivation up to liquid densities corresponding to $Z>10\ \mathrm{ps}^{-1}$. Collisional energy transfer experiments of azulene in binary supercritical xenon/ethane gas mixtures,[25] which at high densities suggest a preferential solvation of azulene with xenon, strongly supported these ideas.

The simple collision model implies that the energy transfer rate constant k_c in a dense environment is directly proportional to the ''coverage'' of the excited molecule by collision partners. If one relates this quantity to the local density, one may in turn try to relate k_c to other observables which also probe the immediate surrounding of the solute. An observable of this kind, e.g., can be the solvatochromic shift of the solute absorption spectrum. Shifts of the azulene $S_3 \leftarrow S_0$ absorption band as a function of the solvent density have been reported already in Ref. 23. As local density variations become even more pronounced in the vicinity of the critical point, we have extended our measurements both of k_c and $\Delta\nu$ into the near-critical range. Propane was used as the solvent for these studies. In this region, the strong density changes related to enhanced cluster formation markedly increase the local density of the solvent around the solute with respect to the bulk, such that parallel effects on energy transfer rates and solvent shift might be expected. Cluster formation leads to large negative solute partial molar volumes of dilute organic solutes in supercritical solvents,[26] and quite generally manifests itself in enhanced solvatochromic shifts of absorption[27] and fluorescence[28] bands of dissolved organic probe molecules. Theoretically it was treated using fluctuation theory.[29] Molecular dynamics simulations[30] with Lennard-Jones fluids under near-critical conditions confirmed that the solute environment is changed with respect to the bulk, but the identity of the solvent molecules in the cluster changes frequently. Recently, the vibrational relaxation time of a single excited carbonyl mode in $W(CO)_6$ was found to be anomalously short in supercritical CO_2 near to the critical point.[31] This observation was interpreted in terms of enhanced cluster formation and related to local density effects as they are manifest also in spectral properties.

In the present work we extended our earlier experiments to broader pressure ranges and to temperatures closer to and more distant from the critical temperature. We show that k_c indeed is closely related to the local solvent density such as expressed by solvatochromic shifts $\Delta\nu$ of the azulene $S_3 \leftarrow S_0$ absorption band. The observed density dependence of the collisional energy transfer process suggests that isolated binary collision (IBC) models can be used, if one expresses the collision frequency Z in terms of the radial distribution function $g(r)$ around the solute. Simulating solute–solvent interactions by an attractive hard-sphere potential, we determined $g(r)$ in Monte Carlo simulations and were able to reproduce the entire density and temperature dependence of k_c in the framework of the IBC model. This implies that only Z is influenced by density but not the average energy transferred per collision $\langle \Delta E \rangle$, which would be the same in the gas as in the liquid phase. Expressing the solvent shift of electronic levels by means of $g(r)$, the density dependence of $\Delta\nu$ can also be described in detail.

II. EXPERIMENTAL TECHNIQUE

In our experiments azulene with a vibrational energy between 19 000 and 20 500 cm^{-1} was generated by laser excitation into the S_1 state and subsequent internal conversion to the S_0 electronic ground state; the preparation of the S_0^* states is achieved within 1 ps.[32] The loss of vibrational energy was monitored on the red wing of the $S_3 \leftarrow S_0$ transition by probe pulses at a wavelength of 290 nm. The energy dependence of absorption coefficients ϵ in this part of the azulene spectrum is well characterized (see below), allowing for a conversion of transient absorption signals into energy decay curves.

For experiments at high bath gas densities (>0.5 mol/ℓ), the required pump and probe pulses were generated with a colliding pulse mode-locked dye laser. Its output pulses at a wavelength of 620 nm were amplified in a three stage Nd:YAG laser pumped dye amplifier[33] to energies of $\sim$140 μJ. After recompression and focusing part of the energy into a 1 cm water cell generating a white light continuum, an interference filter was used to select the desired pump light at 580 nm which was amplified in two subsequent Rhodamine 6G dye cells. The probe wavelength of 290 nm was generated by frequency doubling part of the light in a potassium dihydrogen phosphate (KDP) crystal. Excitation and probe energies were $\sim$60 and 2 μJ, respectively. Both laser pulses were fed into a standard pump-and-probe interferometer, recombined, and collinearly focused into the sample cell. The relative plane of polarization was adjusted to 54.7°. Probe energies were determined in front of and behind the sample cell by means of photodiodes. Behind the sample, an interference filter for the probe wavelength was used to block transmitted excitation light. The width of the cross correlation of pump and probe laser pulses was $\Delta\tau=0.65$ ps (full width at half maximum), i.e., adequate to monitor all processes following the 1 ps preparation of excited states.

Experiments at high densities with bath gas pressures up to 1000 bars and temperatures between 298 and 640 K were performed in a heatable high pressure cell with an optical path length of 20 mm. Sapphire windows with a thickness of 10 mm and an aperture of 7 mm were used. Temperatures were determined with an accuracy of 0.2 K. The precision in determining pressures below 100 bars was 0.1 bar; at higher pressures, it was 1%. Azulene concentrations were adjusted to an optical density of 1.0–1.5 at 290 nm (corresponding to 2×10^{-4} mol/ℓ) which was sufficient to avoid azulene–azulene collisions during the collisional deactivation process.

For low pressure experiments, pulses from a frequency doubled Nd:YAG laser at a wavelength of 532 nm were used for excitation. The 290 nm probe wavelength was obtained by second harmonic generation of the output of a Rhodamine 6G dye laser operating at 580 nm, which was pumped by a second frequency doubled Nd:YAG laser. The delay between pump-and-probe pulses was adjusted by an electronic delay generator (DG 535, Stanford Research Systems). The pump pulses had energies of about 25 mJ. The pulses in a collimated beam of 7 mm width entered a heatable sample cell having an optical path length of 20 cm. The probe beam

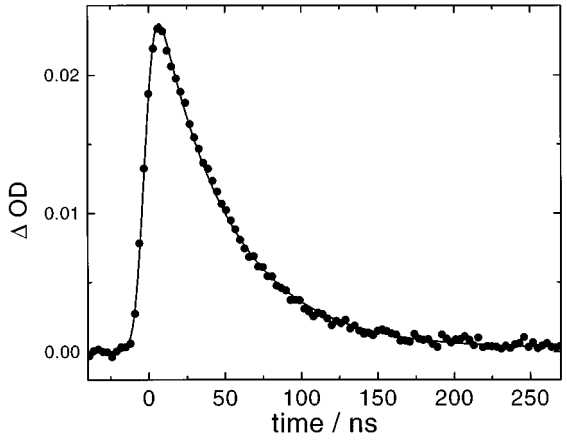

FIG. 1. Absorption time profile recorded during the collisional deactivation of azulene in propane at 391.2 K, 39.5 mbars (full line: simulation assuming an exponential energy decay).

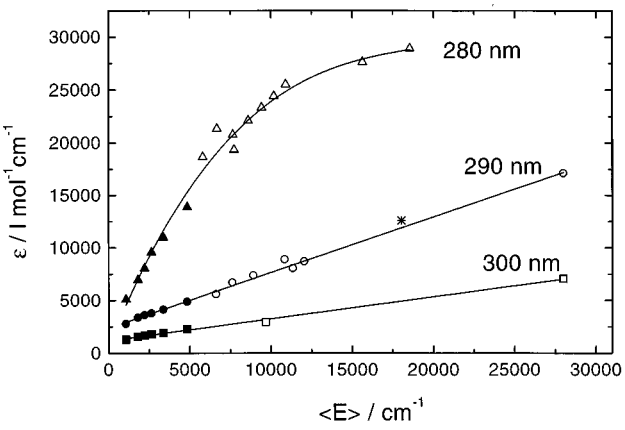

FIG. 2. Energy dependence of azulene absorption coefficients in the gas phase at selected wavelengths. Filled symbols: from static gas cell (Ref. 23); open symbols: from shock wave experiments (Ref. 34); (*) from laser excitation experiments (Ref. 34).

of 3 mm width passed the cell in opposite direction. Pulse energies (near 5 μJ) were detected in front of and behind the sample cell. The low pressure cell was filled with 80–100 μbars of azulene and, depending on the energy transfer efficiency, 30–100 mbars of collider gas. Pressures were determined with an accuracy of 0.5%. The time resolution in these experiments was 8 ns.

Solvent shifts of the azulene $S_3 \leftarrow S_0$ absorption band were determined in a Varian Cary 5E spectrometer under the same conditions as in the time resolved experiments. Azulene (Merck >98% pure) and high purity gases (Messer–Griesheim) and liquids (Barker) were used without further purification.

III. RESULTS

A. Low pressure experiments

In agreement with our earlier work,[23] transient signals of azulene recorded at 290 nm at densities below 1 mol/ℓ were found to decay exponentially. A typical signal from our low pressure experiments is shown in Fig. 1 (bath gas propane at 39.5 mbars and 391.2 K). Decreasing the excitation intensity lowers the amplitude of the signals but has no influence on the decay rate of the signals, indicating that possible two-photon effects can be neglected. Since the energy dependence of the absorption coefficient ϵ at 290 nm is linear (see Fig. 2), energy-loss profiles of the form

$$\langle E(t)\rangle = \langle E_0\rangle \exp(-t/\tau_c) = \langle E_0\rangle \exp(-k_c t), \tag{1}$$

convoluted with a Gaussian instrument response function of 8 ns width, were fitted to the data (solid line in Fig. 1); $\langle E_0\rangle$ denotes the photon energy of the excitation pulse and τ_c is a phenomenological relaxation time constant. It was shown[10] that the slope of the energy decay curves gives direct access to average energies $\langle \Delta E\rangle$ transferred per coillision through

$$d\langle E\rangle/dt = Z\langle \Delta E\rangle, \tag{2}$$

as long as the energy dependence of $\langle \Delta E\rangle$ is not too strong, and the distribution of excited molecules is sufficiently far from the final thermal equilibrium. Combination of Eqs. (1) and (2) gives

$$\langle \Delta E\rangle = -\langle E\rangle/(Z\tau_c); \tag{3}$$

i.e., for an exponentially decaying $\langle E(t)\rangle$ curve, $\langle \Delta E\rangle$ depends linearly on $\langle E\rangle$ with the slope

$$m_{\langle \Delta E\rangle} = \langle \Delta E\rangle/\langle E\rangle = -1/(Z\tau_c) = -k_c/Z. \tag{4}$$

Identifying Z with the Lennard-Jones collision frequency Z_{LJ} and using Lennard-Jones parameters σ=6.61 Å and ϵ/k_B =523 K for azulene and values for the collision partners such as tabulated in Ref. 35, one obtains $m_{\langle \Delta E\rangle}$ in the temperature range 373–391 K such as summarized in Table I. In comparison to extrapolated data from experiments at 385 K and high densities (>0.2 mol/ℓ)[23] these values are larger by 10–25%. Apparently the extrapolation in Ref. 23 slightly underestimated the limiting low pressure values. Earlier dilute gas phase experiments performed at 298 K gave slightly larger $\langle \Delta E\rangle$ than the present results: for propane, e.g., the $m_{\langle \Delta E\rangle}$ value of Table I corresponds to $\langle \Delta E(15\,000\ \mathrm{cm}^{-1})\rangle = -530\ \mathrm{cm}^{-1}$ while the value reported by Hippler *et al.*[6] is $\langle \Delta E(15\,000\ \mathrm{cm}^{-1})\rangle = -640\ \mathrm{cm}^{-1}$ at 298

TABLE I. Average energies $\langle \Delta E\rangle$ of excited azulene transferred per collision. [$m_{\langle \Delta E\rangle} = \langle \Delta E\rangle\langle E\rangle$, see Eq. (4)], and critical parameters for a series of bath gases.

gas	ρ_c (mol ℓ^{-1})	T_c (K)	T (K)	$-100\, m_{\langle \Delta E\rangle}$
xenon	8.454[a]	289.74[a]	375	0.73
CO_2	10.59	304.21	373	1.89
ethane	6.784	305.33	376	2.83
propane	4.966	369.80	391	3.54
n-pentane	3.216[b]	470.60[b]	···	···
n-octane	2.136	568.6	373	8.7

[a]Reference 36.
[b]Reference 43.

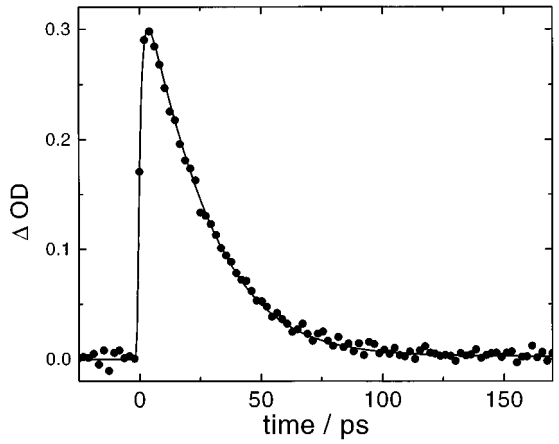

FIG. 3. As Fig. 1, in propane at 372.5 K, 43.6 bars.

K. This difference probably reflects an apparent temperature dependence of $\langle \Delta E \rangle$, if Z is expressed by the Lennard-Jones collision frequency (see below).

B. High pressure experiments

At high densities, the azulene S_3 absorption band increasingly shifts to the red by $\Delta\lambda$ such as discussed in Sec. III C. As a consequence a high density probe wavelength of 290 nm corresponds to a low pressure gas phase probe wavelength of $\lambda_{\text{eff}}=290\ \text{nm}-\Delta\lambda$. Since the energy dependence of the azulene absorption coefficient critically depends on the wavelength (see Fig. 2), the absorption coefficient as a function of the excitation energy $\epsilon(\langle E \rangle)$ was evaluated for λ_{eff} by interpolation between 280 and 290 nm calibration curves. Assuming that Eq. (1) is also valid at higher densities and considering the finite time resolution (due to the internal conversion process and the laser pulse cross correlation width of 0.65 ps), an evaluation function [see Eq. (10) in Ref. 23] was determined and fitted to the data. Even for signals recorded close to the propane critical point (see Fig. 3), where the optical quality of the sample was decreased due to density fluctuations, the agreement between this evaluation function and the signals was excellent, yielding reliable values for τ_c. The derived values for τ_c are summarized in Tables II–IV. Laser intensities used in our picosecond experiments were much higher than in the low pressure experiments. However, possible two-photon excitation leads to azulene in the S_2 state, which at high densities decays much slower than the energy of singly excited molecules in the ground state and, therefore, does not contribute to the signal.

In Fig. 4(a) collisional deactivation rate constants $k_c=\tau_c^{-1}$ are plotted versus propane reduced densities $\rho_r=\rho/\rho_c$, where ρ_c is the critical density of propane (critical parameters are given in Table I). For comparison the extrapolated density dependence of k_c from our low pressure experiments is shown as a solid line. Even at densities as low as $\rho_r=0.17$, our high density data are notably below the extrapolated gas phase behavior. At $\rho_r>0.5$ the initial increase of k_c with density at 396 and 415 K at first becomes slower and at $\rho_r>1.5$ becomes stronger again. Our new results for propane at 396 and 415 K are consistent with earlier results from Ref. 23 for the bath gases CO_2, Xe, and ethane. These results are shown for comparison in Figs. 5(a), 6(a),

TABLE II. Vibrational deactivation times τ_c of azulene in propane at 372.5 K.

p (bars)	ρ (mol ℓ^{-1})[a]	$\Delta\lambda$ (nm)	τ_c (ps)
31.5	1.50	1.8	54
36.3	1.94	2.3	41
36.3	1.94	2.0	42
40.3	2.51	3.5	34
41.5	2.79	4.0	29
42.5	3.11	4.4	25.0
43.2	3.38	4.7	22.0
43.5	3.57	4.8	21.1
43.7	3.73	4.9	20.1
43.9	3.93	5.0	19.9
44.2	4.38	5.1	19.6
46.0	6.44	5.1	17.8
48.2	7.01	5.1	17.6
52.9	7.51	5.2	17.3
60.3	7.97	5.4	16.5
75.5	8.51	5.5	15.6
98.4	9.0	5.8	15.5
135	9.5	6.0	14.8
183	10.0	6.4	14.7
260	10.5	6.7	13.2
357	11.0	6.9	12.8
701	12.1	7.5	11.5

[a]Reference 37.

TABLE III. Vibrational deactivation times τ_c of azulene in propane at 396.5 K.

p (bars)	ρ (mol ℓ^{-1})[a]	$\Delta\lambda$ (nm)	τ_c (ps)
22.8	0.825	1.0	96
37.0	1.57	1.9	59
51.0	2.79	3.1	32
53.0	3.05	3.4	31
55.0	3.35	3.6	28.5
57.0	3.70	3.8	27.2
58.8	4.04	4.0	25.1
61.1	4.50	4.3	24.5
63	4.87	4.5	23.6
65	5.23	4.6	22.5
70	6.0	4.9	21.3
75	6.5	5.0	21.2
81	6.9	5.1	21.0
87	7.3	5.2	20.0
108	8.0	5.4	18.9
130	8.5	5.5	16.8
152	8.8	5.7	16.6
208	9.5	6.0	14.6
275	10.0	6.4	14.0
360	10.5	6.7	13.5
480	11.0	6.9	12.7
618	11.5	7.2	12.2
892	12.2	7.5	11.0

[a]Reference 37.

TABLE IV. Vibrational deactivation times τ_c of azulene in propane at 415 K.

p (bars)	ρ (mol ℓ^{-1})[a]	$\Delta\lambda$ (nm)	τ_c (ps)
72	4.29	4.1	24.5
82	5.37	4.6	22.2
92	6.15	4.9	20.9
120	7.39	5.2	19.5
200	8.85	5.7	16.7

[a]Reference 37.

and 7(a), respectively. These earlier experiments corresponded to situations far above the critical temperatures T_c.

The comparison of measurements in propane at 396 and 414 K with the results at 372.5 K shows large changes at temperatures close to T_c [see Fig. 4(a)]. Contrary to temperatures far above T_c, in propane at 372.5 K (which is 3.4 K above T_c) the increase of k_c with density between $0.5<\rho<1.5$ first becomes stronger and then levels off, reaching a plateau located around ρ_c where the collisional deactivation rate constants become nearly independent of propane density. The near-critical k_c values at ρ_c are larger by 25% than the 396 and 415 K values. For $\rho_r>1.5$, the density dependences of k_c at 372.5 K coincide with those at 396 and 415 K.

Figure 8(a) demonstrates the density dependence of k_c for *n*-pentane and *n*-octane at $\rho_r>2.5$ (data from Ref. 23).

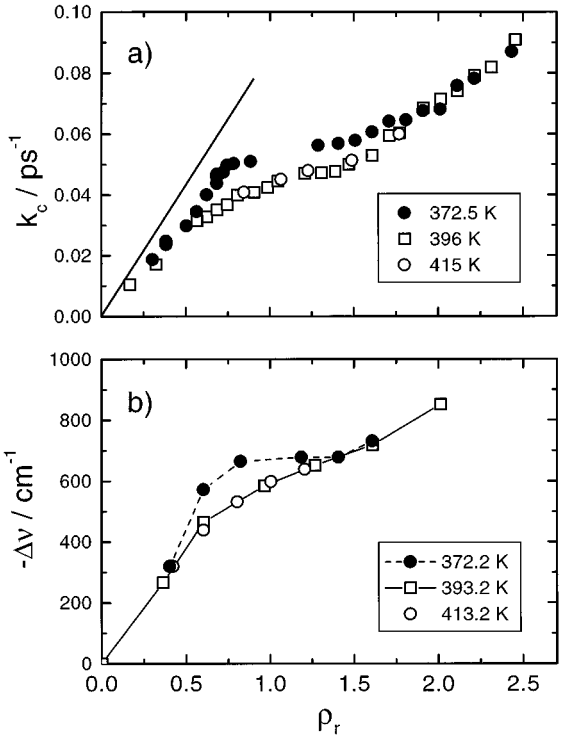

FIG. 4. (a) Density dependence of collisional deactivation rate constants of azulene in propane at various temperatures (full line: extrapolation from dilute gas phase experiments). (b) Density dependence of the shift of the azulene $S_3 \leftarrow S_0$ absorption band in propane at various temperatures.

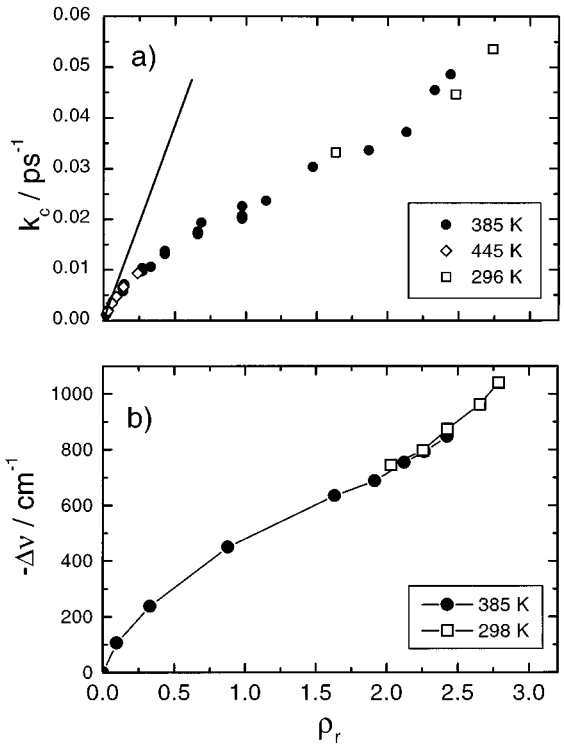

FIG. 5. As Fig. 4, bath gas CO_2.

Clearly, the k_c increase is stronger than proportional to density. This high density behavior is typical and also visible in Fig. 7(a) for ethane. For the bath gas ethane, collisional deactivation rate constants of azulene were determined in the

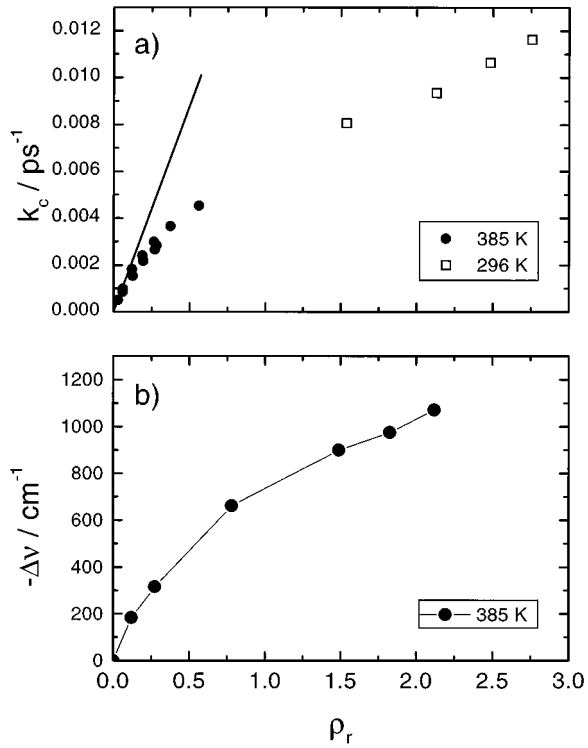

FIG. 6. As Fig. 4, bath gas xenon.

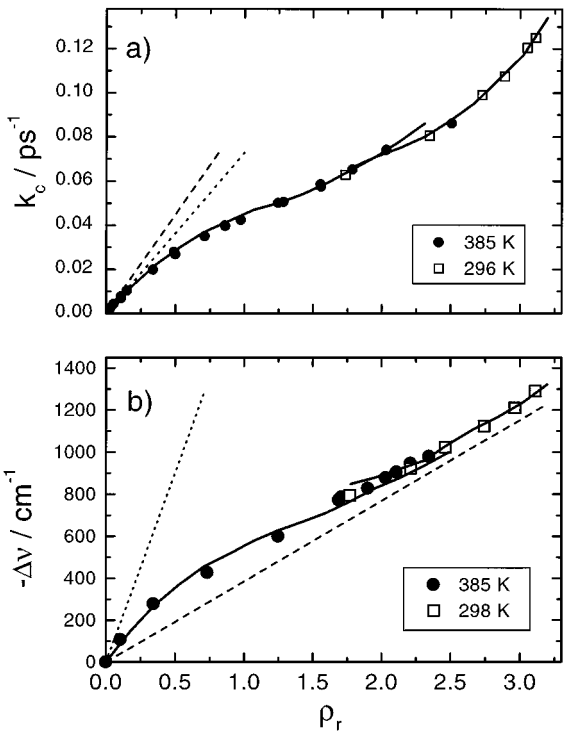

FIG. 7. (a) Density dependence of collisional deactivation rate constants of azulene in ethane (dashed line: extrapolation from dilute gas phase experiments; full lines: attractive hard sphere collision model at 385 and 298 K, respectively; dotted line: extrapolation of the low density limit of the attractive hard sphere collision model, see text). (b) Density dependence of shifts of the azulene $S_3 \leftarrow S_0$ absorption band in ethane. Full lines: simulations at 385 and 298 K, respectively, using Eq. (14); dotted line: reaction-field result with $a=\sigma_u/2$ [Eq. (12)]; dashed line: Abe's result [Eq. (13), see text].

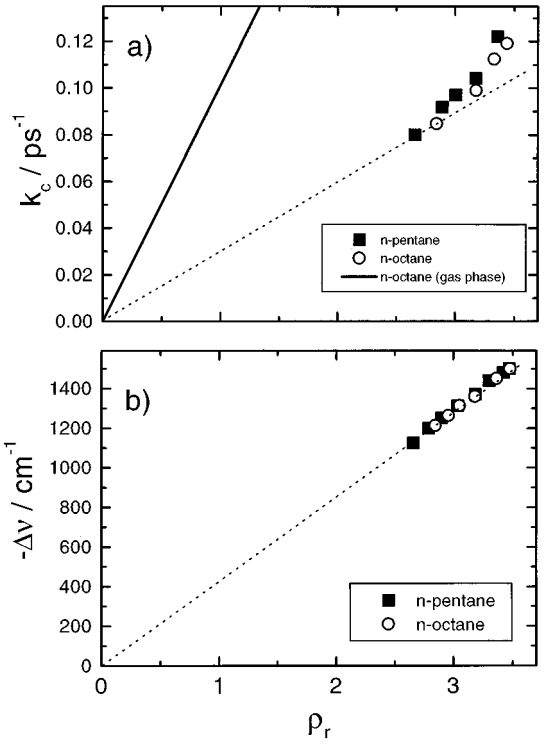

FIG. 8. As Fig. 4, for *n*-pentane and *n*-octane (dotted lines clarify deviations from linear density dependences of the data points).

temperature range 340–640 K at constant densities 2.0 and 11.5 mol/ℓ. The results are summarized in Table V. Figure 9 shows plots of k_c/ρ_r versus temperature for both densities. Whereas at 2 mol/ℓ k_c strongly decreases with temperature, at 11.5 mol/ℓ it nearly remains constant.

C. Comparison of energy transfer and spectral shift data

A comparison of our energy transfer results with measurements of the solvent shifts of the $S_3 \leftarrow S_0$-absorption band under equal temperature and pressure conditions is most illuminating. Figure 4(b) displays shifts $\Delta\nu$ of the azulene $S_3 \leftarrow S_0$-absorption band as a function of the reduced density of propane. The same characteristic features are present as in the energy transfer observations of Fig. 4(a): the 372.2 K curve shows an increase of the low pressure slope at $\rho_r = 0.5$ and then a leveling-off just before the critical density. Around ρ_c essentially no further density shift of the absorption band is observable. At $\rho_r > 1.5$, a slower increase of $\Delta\nu$ with density follows. At higher temperatures (393.2 and 413.2 K), shifts around ρ_c are smaller and the plateau is absent. It should be mentioned that vibrational relaxation from low vibrational states and spectral shifts for the CO stretch mode of $W(CO)_6$ in near-critical CO_2 showed behavior analogous[31] to the present experiments in near-critical propane.

It is important to notice that the density dependences of the energy transfer rate constants k_c and the spectral shifts $\Delta\nu$ are closely related at temperatures very near to T_c as well as more than 40 K away. It is equally important to observe that the behavior is quite general. Figures 5–7 compare k_c and $\Delta\nu$ for the bath gases CO_2, Xe, and ethane at temperatures markedly above T_c where the relation is still observable. Qualitative differences in the density dependence of k_c and $\Delta\nu$ occur only in the compressed liquid. As demon-

TABLE V. Temperature dependence of vibrational deactivation times τ_c of azulene in ethane at densities of 2 and 11.5 mol/ℓ.

p (bars)	T (K)	ρ (mol ℓ$^{-1}$)[a]	Δλ (nm)	τ_c (ps)
43.0	344	1.97	1	50
45.0	353	1.97		50
53.5	385	2.08		55
90	576	1.96		71
102	645	1.99		75
42.5	294	11.5	5	18.0
125	323			17.5
272	373			18.3
418	423			17.7
563	473			16.4
705	523			16.5
846	573			16.5

[a]Reference 38.

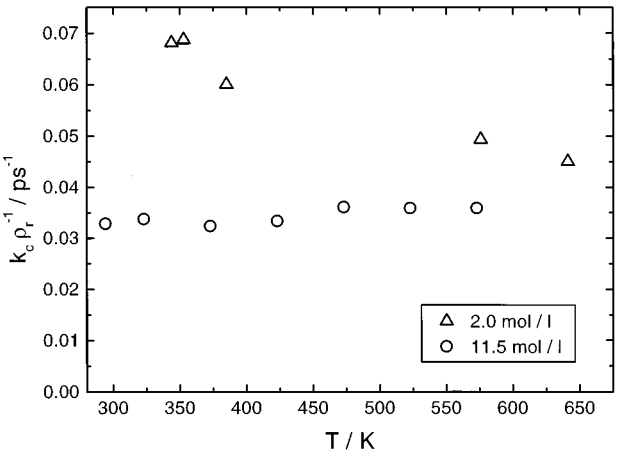

FIG. 9. Temperature dependence of the collisional deactivation rate constant in ethane at various densities (see text).

strated in Fig. 7 for ethane and Fig. 8 for *n*-pentane and *n*-octane, at $\rho_r > 2.5$ k_c increases much stronger with density than $\Delta\nu$.

Before interpreting the density dependences of k_c and $\Delta\nu$, we illustrate the relation between k_c and $\Delta\nu$, in an alternative way. Figures 10 and 11 show k_c as a function of the solvent shift $\Delta\nu$ ($\Delta\nu$ curves were interpolated between the measured points). It is striking that the curves for propane, close to the critical temperature T_c and 40 K above, nearly coincide in Fig. 10. Also, the curves for the other gases in Fig. 11, at temperatures markedly distant from T_c, up to liquid densities are practically linear, however with different slopes. Deviations from linearity occur only at liquid densities, which in Figs. 10 and 11 correspond to solvent shifts of $\Delta\nu > 800\ \mathrm{cm}^{-1}$. This behavior strongly suggests that k_c and $\Delta\nu$ are governed by the same property of the system. Since $\Delta\nu$ is determined by short-range interactions between solute

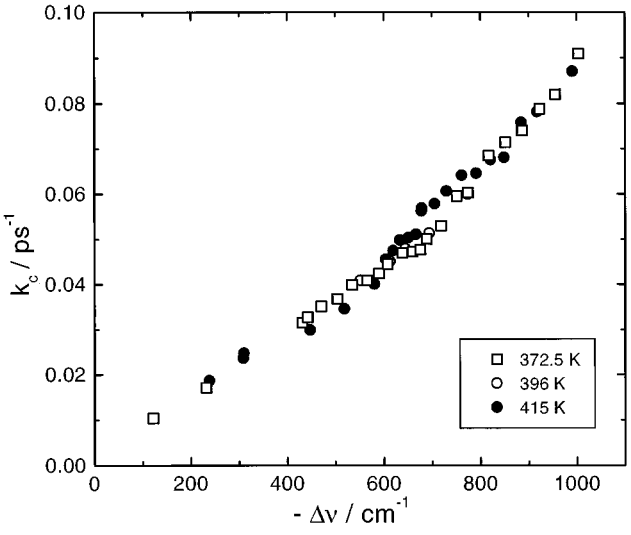

FIG. 10. Relation between the collisional deactivation rate constant k_c and the solvent shift of the spectrum of azulene in propane; see Figs. 4(a) and 4(b).

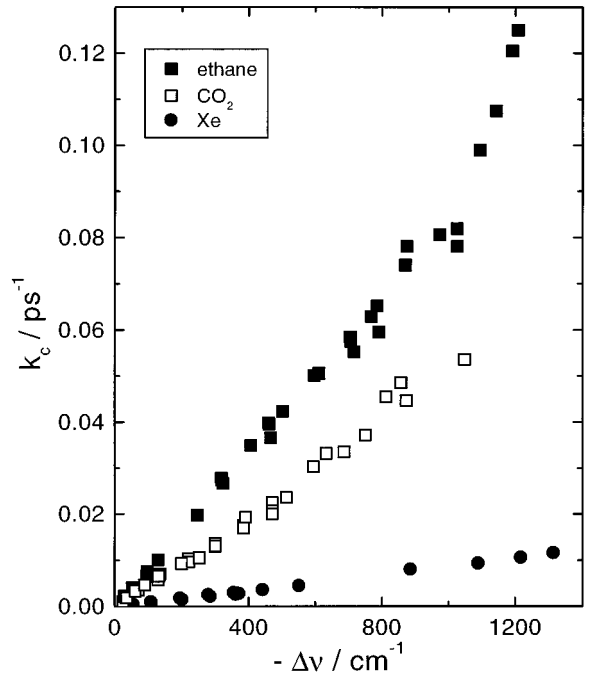

FIG. 11. As Fig. 10, bath gases ethane, CO_2, and xenon.

and bath gas molecules, it seems reasonable to attribute the density dependences both of k_c and $\Delta\nu$ to the local solvent density in the immediate surrounding of the considered solute.

IV. DISCUSSION

In the following we try to relate solvent shifts and collisional deactivation rate constants with local densities such as derived from radial distribution functions of attractive hard-sphere particles in Lennard-Jones fluids.

A. Collisional deactivation rate constants k_c

Early attempts to calculate collision frequencies in dense media were made within the framework of IBC models. Such models were developed to describe the density dependence of vibrational energy relaxation of small molecules, i.e., deactivation of singly excited vibrational modes (see Ref. 39). The basic assumptions of IBC models are that collisional energy relaxation proceeds only via binary interactions and that P, the relaxation probability per collision, is the same for both gas and liquid phase. The rate of relaxation then is given by

$$k(\rho,T) = P(T) \cdot Z(\rho,T). \tag{5}$$

In this model the density dependence of k is exclusively due to that of Z, whereas the temperature influences the vibrational relaxation rate through P and Z. Once P has been found in the gas phase, the determination of k in the liquid reduces to a calculation of the appropriate collision frequency. Defining a collision as an event in which two molecules approach each other to within a certain distance,

which for a hard-sphere solute of diameter σ_u in a hard-sphere solvent of diameter σ_v is given by $\sigma=(\sigma_u+\sigma_v)/2$, the collision frequency is expressed by[40,41]

$$Z=Z_0\cdot g(\rho,T,\sigma), \tag{6}$$

where $g(\rho,T,\sigma)$ is the value of the radial distribution function of the solute at contact with the solvent and Z_0 is the dilute gas collision frequency

$$Z_0=\rho\sigma^2\sqrt{\frac{8\pi k_BT}{\mu}}. \tag{7}$$

Starting from Eq. (6), Delalande and Gale[42] had to add an attractive Lennard-Jones term to the solute–solvent hard-sphere potential in order to model experimental observations on vibrational relaxation rates in liquids.

In the following, we will apply this attractive hard-sphere (AHS) model to the density dependence of collisional energy transfer of vibrationally highly excited azulene. Since the experimental data for the bath gas ethane are most complete, we modeled this system treating ethane–ethane interactions by a Lennard-Jones potential

$$V_v=4\epsilon_v[(\sigma_v/r)^{12}-(\sigma_v/r)^6] \tag{8}$$

with $\epsilon_v/k_B=220$ K.[43] Azulene–ethane interactions were modeled by an AHS potential[42] with

$$\begin{aligned} &V_u=\infty, \quad r<\sigma_u,\\ &V_u=-\epsilon_u, \quad \sigma_u\leqslant r\leqslant 2^{1/6}\sigma_u,\\ &V_u=4\epsilon_u[(\sigma_u/r)^{12}-(\sigma_u/r)^6], \quad r>2^{1/6}\sigma_u. \end{aligned} \tag{9}$$

For simplicity we used a ratio of $\sigma_u/\sigma_v=1$, such that the well depth ϵ_u was the only adjustable parameter for these calculations.

We determined $g(\rho,T,r)$, and consequently $g(\sigma)$ at the surface of the azulene molecule, using the Monte Carlo method.[44,45] Simulations at low densities were performed in a canonical ensemble of 107 solvent spheres and 1 solute sphere in a cubic simulation box with periodic boundary conditions. At high densities, 255 solvent spheres were used. The minimum image convention was used to calculate potential energies; interactions were truncated at half the box length. Starting from an initially face centered cubic structure, after equilibration up to 10^6 trials for each particle were taken to sample the configurational phase space. $g(r)$ around the solute was determined every five trials.

Results for $g(r)$ in Fig. 12 are plotted against the reduced distance $r^*=r/\sigma$ of an AHS particle at $T=385$ K and various Lennard-Jones reduced densities $\rho^*=\rho\sigma^3$. The depth of the potential well for solvent–solute interactions in all calculations presented here was adjusted to $\epsilon_u/k_B=720$ K. This value for ϵ_u turned out to fit best our collisional energy transfer and solvent shift data of azulene in ethane. The solid line corresponds to the low density limit of $g(r)$, being the analytical solution of the equation

$$g(r)=\exp\left(-\frac{V_u(r)}{k_BT}\right). \tag{10}$$

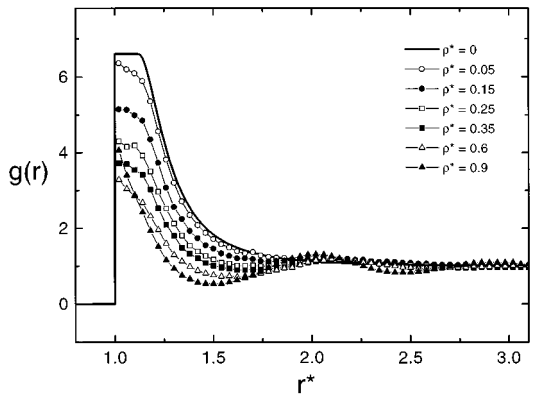

FIG. 12. Radial distribution functions of an attractive hard-sphere particle in a Lennard-Jones fluid at various densities ($\sigma_u=\sigma_v$, $\epsilon_v/k_B=220$ K, $\epsilon_u/k_B=720$ K, $T=385$ K; see text).

At $\rho^*=0.05$, which for supercritical ethane under these conditions corresponds to a pressure of 34 bars, the radial distribution function from our Monte Carlo simulations is still close to this limit. However, around this density the peak at $r^*=1$ begins to decrease. The reason is that the number of molecules in the first solvation shell due to repulsive interactions cannot increase linearly with bulk density. At the same time a second peak around $r^*=2$ grows in, reflecting the formation of a liquid structure. At $\rho^*=0.6$ the peak at $r^*=1$ reaches its minimum. At higher densities the peak increases again and becomes narrower as the molecules in the first shell are forced to stay at the surface of the solute due to repulsive interactions with the remaining solvent. This is the usual behavior in compressed liquids and is independent of the attractive part of the potential.[46] Values of $g(\sigma)$ at the surface of the solute were obtained from $g(r)$ curves in Fig. 12 by extrapolation. Following Eqs. (6) and (7), the collision frequency Z is expected to be proportional to $\rho^*\sqrt{T^*}g(\rho^*,T^*,\sigma)$ with $T^*=k_BT/\epsilon_u$. Figure 13 shows plots of this quantity versus density at 298, 385, and 575 K, respectively. All features, which we observed in the $k_c(\rho)$ dependence of azulene in supercritical fluids more than 20 K above T_c, are present in the 385 K isotherm. The initial

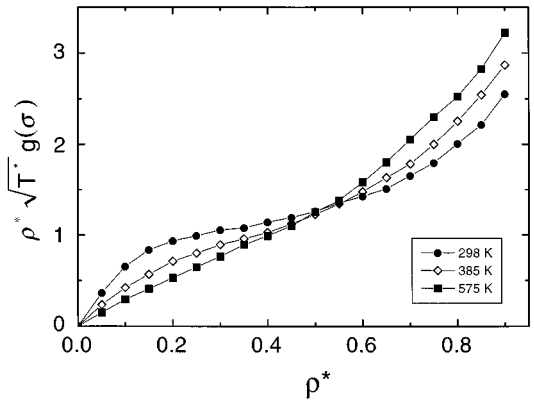

FIG. 13. Density dependence of the reduced collision frequency, Eqs. (6) and (7), at various temperatures (parameters as in Fig. 12).

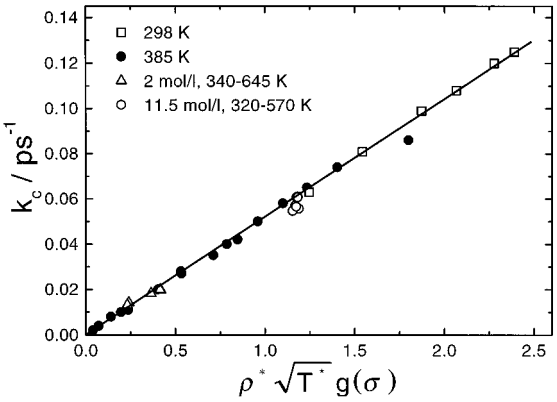

FIG. 14. Collisional deactivation rate constant as a function of the reduced collision frequency, Eqs. (6) and (7), at various densities and temperatures.

increase of Z at low densities becomes weaker already at $\rho^*<0.05$ (see also Fig. 12). At $\rho^*\approx 0.5$ an inflection point is reached, followed by a stronger increase of Z with density. It is possible to directly project the 298 and 385 K isotherms of Fig. 13 to the $k_c(\rho)$ data of azulene in ethane such as demonstrated by full lines in Fig. 7(a). A Lennard-Jones diameter of $\sigma=0.41$ nm for ethane was used to transform ρ^* into ρ_r (values reported in the literature are in the range 0.39–0.44 nm; see Ref. 43). The agreement with the data is excellent; only the limiting low density slope of k_c is slightly underestimated (dotted line). Figure 13 shows that, for constant ρ^*, the collision frequency at low densities strongly decreases with increasing temperature. At $\rho^*=0.5$, however, the temperature dependence of Z is only weak. This behavior agrees with the temperature dependences of k_c such as presented in Fig. 9 (densities of 2.0 and 11.5 mol/ℓ ethane correspond to $\rho^*=0.083$ and 0.48, respectively). Plotting k_c from Figs. 7 and 9 versus $\rho^*\sqrt{T^*}g(\rho^*,T^*,\sigma)$, all data points fall on one straight line such as shown in Fig. 14. This indicates that, within the AHS collision model, deactivation rate constants of azulene in ethane at 298–640 K are determined only by $Z(\rho,T)$, whereas $\langle\Delta E\rangle$ is temperature and density independent.

B. Solvent shifts $\Delta\nu$

The solvent shifts $\Delta\nu$ are caused by weak interactions between the solute and surrounding solvent molecules. The change in energy of the solute due to this interaction will differ depending on whether the molecule is in its ground or excited state. Consequently, a change in excitation energy $\Delta\nu$ will be observed experimentally. Most theoretical approaches to characterize the solvent shift are based on Onsager's reaction-field method derived from classical electrostatics.[47–49] These models consider a point dipole in the center of a spherical cavity (radius a) surrounded by a homogenous dielectric. Here, we follow the model suggested by Abe,[50] who considered van der Waals interactions between two molecules averaged over all orientations.[51] Assuming that solute–solvent interactions consist of pairwise interactions of this type, the stabilization of an electronic state s of the solute is given by[52]

$$\Delta E_s=\sum_{p=1}^{N} R_p^{-6}\left\{-\frac{2}{3k_BT}(\mu_s^u)^2(\mu^v)^2-\alpha_s^u(\mu^v)^2 - \alpha^v(\mu_s^u)^2+d_{uv}^s\right\}, \tag{11}$$

where α and μ denote polarizabilities and dipole moments of solute (index u) and solvent (index v) molecules, respectively. The van der Waals coefficient d_{uv}^s is due to dispersion forces. R_p denotes the distance between the solute and individual solvent molecules, which were assumed to be of spherical symmetry. The reaction-field result is obtained, if a uniform distribution of solvent molecules outside the cavity of radius $a=\sigma_u/2$ is considered:

$$\sum_{n=1}^{\infty} R_p^{-6}=\frac{2^5}{3}\,\pi\,\frac{\rho}{\sigma_u^3}. \tag{12}$$

Abe supposed that the solvent molecules are arranged around the solute in fixed shells, such that the values of R_p are $(\sigma_u/2+\sigma_v/2)$, $(\sigma_u/2+3\sigma_v/2)$, $(\sigma_u/2+5\sigma_v/2)$, etc., and the number of solvent molecules at these distances are $4\pi(\sigma_u/2+\sigma_v/2)^2/\sigma_v^2$, $4\pi(\sigma_u/2+3\sigma_v/2)^2/\sigma_v^2$, etc. If $\sigma_u=\sigma_v$ his final result is

$$\sum_{n=1}^{\infty} R_p^{-6}=\frac{1}{135}\,\pi^6\,\frac{\rho}{\sigma_u^3}. \tag{13}$$

The accurate method to evaluate ΣR_p^{-6}, of course, applies the radial distribution function which gives

$$\sum_{n=1}^{\infty} R_p^{-6}=4\pi\rho\int_0^{\infty}\frac{g(r)}{r^4}\,dr=4\pi\,\frac{\rho}{\sigma_u^3}\int_0^{\infty}\frac{g(r^*)}{r^{*4}}\,dr^*. \tag{14}$$

For nonpolar solvents only dispersion forces and interactions between the solute dipole and induced dipole in the solvent have to be considered. Therefore, the change in energy between ground (index g) and excited (index e) state is

$$\Delta E_{e-g}=4\pi\rho\int_0^{\infty}\frac{g(r)}{r^4}\,dr\{\alpha^v[(\mu_g^u)^2-(\mu_e^u)^2] + d_{uv}^e-d_{uv}^g\}. \tag{15}$$

We applied Eq. (15) to our solvent-shift data of azulene in ethane by taking the expression in brackets as a scaling factor, because the estimation of dispersion terms is unreliable. For consistency, the same radial distribution functions as calculated in 4.1 to fit the $k_c(\rho)$ data were used. The agreement between Eq. (15) and solvent shift is excellent as demonstrated in Fig. 7(b) (solid lines). At high densities the calculated curves turn over to a linear behavior, such that the main difference to the $k_c(\rho)$ data is well reproduced. The reason is that in the range $0.6<\rho^*<0.9$, the value of the radial distribution function $g(\sigma)$ at the surface of the solute increases with density (see Fig. 12); the width of the peak of $g(r)$ at

$r^*=1$, however, narrows simultaneously, such that the integral in expression (14) remains nearly constant. Dotted and dashed lines in Fig. 7(b) represent reaction-field and Abe's result of Eqs. (12) and (13), respectively. The dashed line well reproduces the high density limit of the calculations using $g(r)$, since under these conditions the spherical molecules are nearly arranged as Abe supposed in his model. The reaction field gives too high stabilization energies if the cavity radius a is set to $\sigma_u/2$. A value of $1.67\cdot\sigma_u/2$ instead reproduces the dotted line such as was already noticed in Ref. 52.

C. Collisional deactivation rate constants and solvent shifts close to the critical point

So far we have analyzed the density dependence of k_c and $\Delta\nu$ only well above or below the critical point. Figure 4(a) shows that the collisional deactivation rate of azulene in propane close to T_c is nearly constant in a range $0.75<\rho_r<1.5$. From the parallel behavior of $\Delta\nu(\rho)$ under these conditions [see Fig. 4(c)], one has to conclude that again the local density determines the anomalous $k_c(\rho)$ dependence, and that the energy transfer mechanism does not change. Debenedetti investigated solute–solvent properties at infinite dilution in the vicinity of the solvent's critical point by means of fluctuation analysis.[29] Defining a cluster size in terms of statistical correlations between solute and solvent concentration fluctuations, he showed that closely above T_c the excess number of solvent molecules surrounding a given attractive solute molecule strongly increases, with respect to a uniform distribution at the prevailing density. Calculations, which were based on measured infinite dilution solute partial molar volume of naphthalene in CO_2 at 4 K above T_c:[26c] show an increase of the cluster size in the range $\rho_r=0.7-0.9$ from 20 to 100 solvent molecules (cf. Fig. 1 in Ref. 29) and a subsequent decay to 10 solvent molecules when the density is further raised to $\rho_r=1.2$. The density region where these large clusters exist agrees approximately with the range of constant $\Delta\nu(\rho)$ and $k_c(\rho)$ in Fig. 4. It is conceivable that, while these clusters exist, the density at the surface of the solute molecule does not change and, therefore, $\Delta\nu$ and k_c remain constant. Unfortunately, this effect cannot be reproduced by Monte Carlo simulations of the type used in the present work, because the limited number of molecules in a simulation box with periodic boundary conditions prevents the formation of density fluctuations of the size reported in Ref. 29.

V. CONCLUSIONS

The comparison with shifts of electronic absorption spectra suggests that collisional energy transfer rates of highly excited azulene are determined by the local bath gas densities. Therefore, the density dependence of k_c was described within the framework of an IBC model which relates the collision frequency to the value of the radial distribution function $g(r)$ at the surface of the solute molecule. Applying simple interaction potentials, $g(\rho,T,r)$ was calculated by Monte Carlo simulations of a canonical ensemble. The same radial distribution functions were used to describe the stabilization of electronic states of a solute in the presence of solvent molecules. Both models very successfully describe $k_c(\rho)$ and $\Delta\nu(\rho)$ if the temperature is not too close to the solvent's critical temperature T_c. Close to T_c, the (constant NVT) Monte Carlo method with a small number of molecules fails to correctly describe the long range fluctuations present under near-critical conditions. In order to improve the simulations of $k_c(\rho)$ and $\Delta\nu(\rho)$ for temperatures near to T_c, we currently implement the Gibbs Monte Carlo technique.[53] The IBC approach in the applied form is an extension of the simple adsorption model presented in Ref. 23 because many-body effects present at high densities are explicitly considered through $g(r)$.

Our investigations clearly show that the density and temperature dependences of the collisional deactivation rate constants of highly excited azulene can satisfactorily be explained by local density influences on binary collision numbers. As a consequence, average energies $\langle\Delta E\rangle$ transferred per collision have to be assumed to be practically independent of pressure and temperature and, therefore, are identical for gas and liquid phase conditions. Classical trajectory calculations of $\langle\Delta E\rangle$, which quantitatively reproduced experimental values for low pressure gases,[14] hence should also provide a realistic picture for dense fluids. On the other hand, the calculation of collision frequencies should account for local density effects such as demonstrated in the present work.

ACKNOWLEDGMENTS

We would like to thank B. Abel for providing the nanosecond dye laser. Discussions of this work with J. Schroeder, P. Vöhringer, K. Luther, and M. Teubner, as well as financial support by the Deutsche Forschungsgemeinschaft (Sonderforschungsbereich 357 ''Molekulare Mechanismen unimolekularer Prozesse'') are gratefully acknowledged.

[1] M. Quack and J. Troe, in *Gas Kinetics and Energy Transfer*, edited by P. G. Ashmore and R. J. Donovan (The Chemical Society, London, 1977), Vol. 2, p. 175; H. Hippler and J. Troe, in *Bimolecular Collisions*, edited by M. N. R. Ashfold and J. E. Baggott (The Royal Society of Chemistry, London, 1989), p. 209.
[2] D. C. Tardy and B. S. Rabinovitch, Chem. Rev. **77**, 396 (1977); I. Oref and D. C. Tardy, *ibid*. **90**, 1407 (1990).
[3] H. Hippler, J. Troe, and H. J. Wendelken, Chem. Phys. Lett. **84**, 257 (1981); J. Chem. Phys. **78**, 6709 (1983).
[4] H. Hippler, K. Luther, and J. Troe, J. Chem. Phys. **78**, 6718 (1983); M. Damm, H. Hippler, and J. Troe, *ibid.* **88**, 3564 (1988).
[5] M. Heymann, H. Hippler, D. Nahr, H. J. Plach, and J. Troe, J. Phys. Chem. **92**, 5507 (1988); J. E. Dove, H. Hippler, H. J. Plach, and J. Troe, J. Chem. Phys. **81**, 1209 (1984).
[6] H. Hippler, B. Otto, and J. Troe, Ber. Bunsenges. Phys. Chem. **93**, 428 (1989).
[7] G. P. Smith and J. R. Barker, Chem. Phys. Lett. **78**, 253 (1981); J. Shi, D. Bernfeld, and J. R. Barker, J. Chem. Phys. **88**, 6211 (1988); J. Shi and J. R. Barker, *ibid*. **88**, 6219 (1988).
[8] B. M. Toselli, J. D. Brenner, M. L. Yarram, W. E. Chin, K. D. King, and J. R. Barker, J. Chem. Phys. **95**, 176 (1991).
[9] U. Hold, T. Lenzer, K. Luther, K. Reihs, and A. Symonds. Ber. Bunsenges. Phys. Chem. **101**, 552 (1997).

[10] J. Troe, J. Chem. Phys. **77**, 3485 (1982); J. R. Barker, J. Phys. Chem. **88**, 11 (1984).
[11] K. F. Lim and R. G. Gilbert, J. Chem. Phys. **80**, 5501 (1984); **84**, 6129 (1986).
[12] A. J. Stace and J. N. Murrell, J. Chem. Phys. **68**, 3028 (1978); N. J. Brown and J. A. Miller, *ibid*. **80**, 5568 (1984): H. Hippler, H. W. Schranz, and J. Troe, J. Phys. Chem. **40**, 6158 (1986).
[13] M. Bruehl and G. Schatz, J. Phys. Chem. **42**, 7223 (1988).
[14] Th. Lenzer, K. Luther, J. Troe, R. G. Gilbert, and K. F. Lim, J. Chem. Phys. **103**, 626 (1995).
[15] F. Wondrazek, A. Seilmeier, and W. Kaiser, Chem. Phys. Lett. **104**, 121 (1984).
[16] A. Seilmeier, P. O. J. Scherer, and W. Kaiser, Chem. Phys. Lett. **105**, 140 (1984).
[17] U. Sukowski, A. Seilmeier, T. Elsaesser, and S. F. Fischer, J. Chem. Phys. **93**, 4094 (1990).
[18] H. Miyasaka, M. Hagihara, T. Okada, and N. Mataga, Chem. Phys. Lett. **188**, 259 (1992).
[19] K. E. Schultz, D. J. Russel, and C. B. Harris, J. Chem. Phys. **97**, 5431 (1992).
[20] R. J. Sension, S. T. Repinec, A. Z. Szarka, and R. M. Hochstrasser, J. Chem. Phys. **98**, 6291 (1993).
[21] K. Lenz, M. Pfeiffer, A. Lau, and T. Elsaesser, Chem. Phys. Lett. **229**, 340 (1994).
[22] T. Elsaesser and W. Kaiser, Annu. Rev. Phys. Chem. **42**, 83 (1991).
[23] D. Schwarzer, J. Troe, M. Votsmeier, and M. Zerezke, J. Chem. Phys. **105**, 3121 (1996).
[24] J. Benzler, S. Linkersdörfer, and K. Luther, Ber. Bunsenges. Phys. Chem. **100**, 1252 (1996).
[25] D. Schwarzer, J. Troe, M. Votsmeier, and M. Zerezke, Ber. Bunsenges. Phys. Chem. **101**, 595 (1997).
[26] (a) C. A. Eckert, D. H. Ziger, K. P. Johnston, and T. K. Ellison, Fluid Phase Equilibria **14**, 167 (1983); (b) C. A. Eckert, D. H. Ziger, K. P. Johnston, and S. Kim, J. Phys. Chem. **90**, 2738 (1986).
[27] S. Kim and K. P. Johnston, Ind. Eng. Chem. Res. **26**, 1206 (1987); G. E. Bennett and K. P. Johnston, J. Phys. Chem. **98**, 441 (1994); O. Kajimoto, M. Futakami, T. Kobayashi, and K. Yamasaki, ibid. **92**, 1347 (1988); A. Morita and O. Kajimoto, *ibid*. **94**, 6420 (1990).
[28] Y. Sun, G. Bennett, K. P. Johnston, and M. A. Fox, J. Phys. Chem. **96**, 10001 (1992).
[29] P. G. Debenedetti, Chem. Eng. Sci. **42**, 2203 (1987).
[30] I. B. Petsche and P. G. Debenedetti, J. Chem. Phys **91**, 7075 (1989).
[31] R. S. Urdahl, K. D. Rector, D. J. Myers, P. H. Davis, and M. D. Fayer, J. Chem. Phys. **105**, 8973 (1996).
[32] D. Schwarzer, J. Troe, and J. Schroeder, Ber. Bunsenges. Phys. Chem. **95**, 933 (1991); B. D. Wagner, M. Szymanski, and R. P. Steer, J. Chem. Phys. **98**, 301 (1993).
[33] Th. Bultmann, D. Bingemann, N. Ernsting, D. Schwarzer, and L. Nikowa, Rev. Sci. Instrum. **66**, 4393 (1995).
[34] L. Brouwer, H. Hippler, L. Lindemann, and J. Troe, J. Phys. Chem. **89**, 4608 (1985).
[35] H. Hippler, L. Lindemann, and J. Troe, J. Chem. Phys. **83**, 3906 (1985).
[36] Messer Griesheim, *Physical Properties of Gases*, Sach-Nr. 0.812.251, ed. 8109/VII.
[37] B. A. Younglove and J. F. Ely, J. Phys. Chem. Ref. Data **16**, 577 (1987).
[38] D. G. Friend, H. Ingham, and J. F. Ely, J. Phys. Chem. Ref. Data **20**, 257 (1991).
[39] J. Chesnoy and G. M. Gale, Ann. Phys. (Paris) **9**, 893 (1984).
[40] T. Einwohner and B. J. Alder, J. Chem. Phys. **49**, 1458 (1968).
[41] P. K. Davis and I. Oppenheim, J. Chem. Phys. **57**, 505 (1972).
[42] C. Delalande and G. M. Gale, J. Chem. Phys. **71**, 4804 (1979).
[43] R. C. Reid, J. M. Prausnitz, and T. K. Sherwood, *The Properties of Gases and Liquids*, 3rd ed. (McGraw-Hill, New York, 1977).
[44] N. Metropolis, A. W. Rosenbluth, M. N. Rosenbluth, A. H. Teller, and E. Teller, J. Chem. Phys. **21**, 1087 (1953).
[45] M. P. Allen and D. J. Tildesley, *Computer Simulations of Liquids* (Oxford University Press, Oxford, 1987).
[46] D. A. McQuarrie *Statistical Mechanics* (Harper & Row, New York, 1973).
[47] E. G. McRae, J. Phys. Chem. **61**, 562 (1957).
[48] E. Lippert, Ber. Bunsenges. Phys. Chem. **61**, 562 (1957)
[49] W. Liptay, in *Modern Quantum Chemistry*, edited by O. Sinanoglu (Academic, New York, 1966), Part II, p. 173.
[50] T. Abe, Bull. Chem. Soc. Jpn. **38**, 1314 (1965).
[51] H. Margenau, Rev. Mod. Phys. **11**, 1 (1939).
[52] A. T. Amos and B. L. Burrows, Adv. Quantum Chem. **7**, 289 (1973).
[53] A. Z. Panagiotopoulos, Mol. Phys. **61**, 813 (1987).